UDC 551.501.75:519.2 5

# Optimum Interpolation From Observations of Mixed Quality [1]

**MIKHAIL A. ALAKA and ROBERT C. ELVANDER**—*Techniques Development Laboratory, NOAA, Silver Spring, Md.*

**ABSTRACT**—On the basis of a 10-yr record of rawinsonde observations in the Tropics, experiments were run to illustrate the manner in which climatology may be used to minimize the root-mean-square errors of interpolation from data of mixed quality that are irregularly located in time and space. The procedure, based on the theory of optimum interpolation, determines the relative weights of the data used in the interpolation on the basis of their error characteristics, their location, and the scale and variability of the meteorological fields that they sample.

## 1. INTRODUCTION

Meteorological observations over the globe are made from a large variety of platforms and are different in quality and character. With the progressively increasing availability and improvement of observations from satellites and other nonconventional platforms, and the difficulty and expense of greatly increasing the number of conventional radiosonde observations over the oceans and deserts, one can foresee that global meteorological observations of the future will be even more heterogeneous and irregular than they now are.

An "analysis" that would generate, from such an array of observations, a regular three-dimensional lattice of data representing an instantaneous state of the atmosphere must involve interpolation procedures. For best results, of course, these procedures should not be haphazard but rather should aim to extract the maximum information from all available observations and combine these observations, each with its proper weight, to generate the most accurate gridpoint values possible.

Most analysis procedures impose consistency constraints to reduce errors. These constraints are all the more necessary where the observations are sparse or are subject to errors. The constraints imposed may be simple such as the hydrostatic or geostrophic relationships, or they may be complex such as those formulated by Sasaki (1969), Thompson (1969), and others.

In recent years, the theory of optimum interpolation which, by imposing climatological constraints, minimizes the root-mean-square (rms) interpolation errors (Gandin 1963) has attracted increasing attention. Application of this theory requires a knowledge of not only the statistical structure, in time and space, of the meteorological fields that are being analyzed but also of the random errors inherent in the data used in the analysis.

On the basis of a 10-yr record of rawinsonde observations from some 35 stations in the Caribbean region, we have carried out some experiments to illustrate the capability of this method which, under certain circumstances, can generate interpolated gridpoint values with an rms error less than that of the observations themselves. The experiments demonstrate how observations of mixed quality, which may be irregularly located in space and time, can be combined and their optimum relative weights determined on the basis of their error characteristics and their location, as well as the scale and variability of the meteorological fields that they sample. The experiments also shed some light on the usefulness and advantages of forecasts as a first guess and the proper relative weight that they should be given. Finally, the experiments provide some insight into the proper spacing of observations in the Tropics.

[1] Paper presented at the International Symposium on Four-Dimensional Data Assimilation for GARP, Apr. 19–22, 1971, Princeton, N.J.

## 2. BASIC EQUATIONS

Let $\mathbf{r}_i=\mathbf{r}_0, \mathbf{r}_1, \ldots, \mathbf{r}_n$ denote a set of independent vectors defining the location of points in a sampling space. Consider a function $f(\mathbf{r})$ whose sampled values $\hat{f}_i=\hat{f}_1, \hat{f}_2, \ldots, \hat{f}_n$ have errors $\epsilon_i=\epsilon_1, \epsilon_2, \ldots, \epsilon_n$ so that

$$\hat{f}_i=f_i+\epsilon_i. \tag{1}$$

We wish to determine the value $f_0$ at some location $\mathbf{r}_0$ from the measured values $\hat{f}_i$. If $f_0'$ and $f_i'$ denote the deviations of $f_0$ and $f_i$ from their respective means, we may express $f_0'$ in terms of the following linear combination:

$$f_0'=\sum_{i=1}^{n}(f_i'+\epsilon_i)P_i+I_0 \tag{2}$$

in which $P_i$ are the weighting factors and $I_0$ is the error in determining $f_0'$ by interpolation from $\hat{f}_i$.

The mean-square interpolation error is given by

$$\varepsilon=\overline{I_0^2}=\overline{\left[\sum_{i=1}^{n}(f_i'+\epsilon_i)P_i-f_0'\right]^2}. \tag{3}$$

We make the usually satisfactory assumption that the random errors, $\epsilon_i$, are (1) unrelated to the true values of the measured quantities; that is,

$$\overline{\epsilon_i f_i'}=0, \tag{4}$$

and (2) unrelated to each other; that is,

$$\overline{\epsilon_i \epsilon_j}=\begin{cases}0 \text{ when } i\neq j\\ \sigma_{\epsilon_i}^2 \text{ when } i=j\end{cases} \tag{5}$$

where $\sigma_{\epsilon_i}^2$ denotes the mean-square random observation errors. The above assumptions imply that the random errors do not affect the values of the true covariances but inflate the true variances $\sigma_i^2$ by an amount $\sigma_{\epsilon_i}^2$.

By invoking the assumptions in eq (4) and (5), we can rewrite eq (3) as

$$\varepsilon=\sum_{i=1}^{n}\sum_{j=1}^{n}\overline{\hat{f}_i'\hat{f}_j'}P_iP_j+\sum_{i=1}^{n}\sigma_{\epsilon_i}^2P_i^2-2\sum_{i=1}^{n}\overline{\hat{f}_i'f_0'}P_i+\sigma_0^2. \tag{6}$$

The optimum weights, $p_i$, corresponding to a minimum value of $\varepsilon$, are obtained by setting

$$\frac{\partial\varepsilon}{\partial P_i}=0. \tag{7}$$

They form a system of linear equations; that is,

$$\sum_{j=1}^{n}\overline{\hat{f}_i'\hat{f}_j'}p_j+\sigma_{\epsilon_i}^2p_i=\overline{\hat{f}_i'f_0'} \qquad (i=1, 2, \ldots, n). \tag{8}$$

Denoting $\varepsilon_{\min}$ by $E$ and combining eq (6) and (8), we have

$$E=\sigma_0^2-\sum_{i=1}^{n}\overline{\hat{f}_i'f_0'}p_i. \tag{9}$$

It is convenient to assume that the variances are homogeneous and the covariances both homogeneous and isotropic. Equations (8) and (9) may then be written

$$\sum_{j=1}^{n}\mu_{i,j}p_j+\lambda_i^2p_i=\mu_{0,i} \qquad (i=1, \ldots, n) \tag{10}$$

and

$$E=\sigma^2\left(1-\sum_{i=1}^{n}\mu_{0,i}p_i\right) \tag{11}$$

where

$$\mu_{i,j}=\frac{\overline{\hat{f}_i'\hat{f}_j'}}{\sigma^2}$$

is the autocorrelation coefficient between values of the function at locations $\mathbf{r}_i$ and $\mathbf{r}_j$,

$$\mu_{0,i}=\frac{\overline{f_0'\hat{f}_i'}}{\sigma^2}$$

is the autocorrelation coefficient between values of the function at $\mathbf{r}_0$ and $\mathbf{r}_i$, and

$$\lambda_i^2=\frac{\sigma_{\epsilon i}^2}{\sigma^2}.$$

From eq (10) and (11), we note that both the weights and the rms interpolation errors depend on the scale of the function as represented by the autocorrelations $\mu_{0,i}$ and $\mu_{i,j}$, on the variability as represented by $\sigma^2$, and on the random error, $\sigma\epsilon_i$. Equation (11) shows that the mean-square interpolation error cannot exceed the variance of the function that is being interpolated.

## 3. COMPUTATIONAL PROCEDURES

Effective minimization of the rms interpolation error

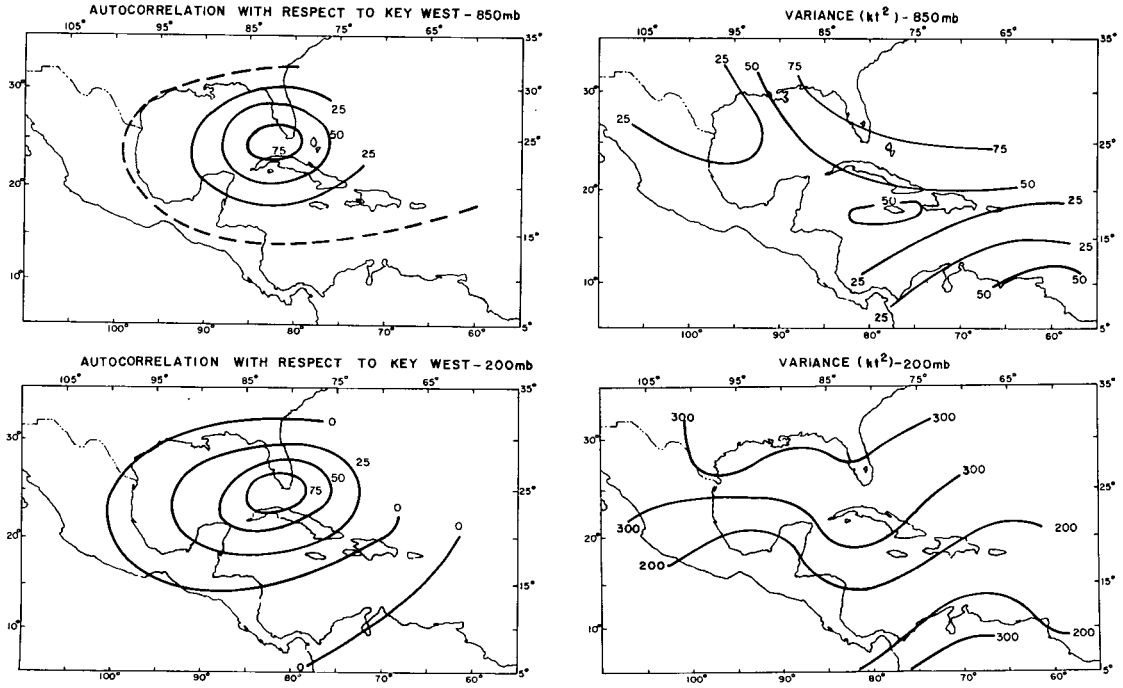


FIGURE 1.—Autocorrelations (in hundredths) and variances of the zonal wind in July.

by the above procedure depends on an accurate estimate of the random errors, the variances, and the autocorrelation functions. We mentioned in the previous section that we have assumed the variances to be homogeneous and the covariances both homogeneous and isotropic.

TABLE 1.—*Estimates of random errors and average variances of the Caribbean data*

| Element | Month | Level (mb) | Rms random error ($\sigma_\epsilon$) | Variance ($\sigma^2$) |
|---|---|---|---|---|
| Zonal wind component ($U$) | January | 850 | 3.0 kt | 84.9 kt$^2$ |
| | | 500 | 4.7 | 244.0 |
| | | 200 | 7.1 | 579.0 |
| | July | 850 | 3.0 kt | 34.3 kt$^2$ |
| | | 500 | 4.0 | 45.5 |
| | | 200 | 4.8 | 241.0 |
| Meridional wind component ($V$) | January | 850 | 3.0 kt | 101.0 kt$^2$ |
| | | 500 | 4.7 | 194.0 |
| | | 200 | 7.1 | 524.0 |
| | July | 850 | 3.0 kt | 29.9 kt$^2$ |
| | | 500 | 4.0 | 34.2 |
| | | 200 | 4.8 | 172.0 |
| Temperature ($T$) | January | 850 | 0.84°C | 10.3°C$^2$ |
| | | 500 | 0.84° | 5.6 |
| | | 200 | 0.84° | 7.1 |
| | July | 850 | 0.84°C | 2.82°C$^2$ |
| | | 500 | 0.84° | 2.03 |
| | | 200 | 0.84° | 3.99 |

Figure 1 indicates that neither assumption is strictly valid. Therefore, due allowance must be made for these assumptions in interpreting our results.

## a. Random Errors

To determine the rms random error, $\sigma_\epsilon$, we have also assumed the structure function, $\beta$, to be homogeneous and isotropic. Under these assumptions, this function depends only on $\rho=\mathbf{r}_i-\mathbf{r}_j$, the distance between observation pairs located at $\mathbf{r}_i$ and $\mathbf{r}_j$. Thus,

$$\beta(\rho)=\overline{(f_i'-f_j')^2}. \tag{12}$$

As shown by Gandin (1963, ch. 2), the estimated structure function $\hat{\beta}(\rho)$ is related to the true function $\beta(\rho)$ as follows:

$$\hat{\beta}(\rho)=\beta(\rho)+2\sigma_\epsilon^2. \tag{13}$$

Thus, $2\sigma_\epsilon^2$ may be estimated by fitting a curve to the computed structure function, $\beta(\rho)$, plotted against distance, $\rho$, and extrapolating the curve until it intersects the axis of $\hat{\beta}(\rho)$ at $\rho=0$. The value of $\sigma_\epsilon^2$ thus estimated will comprise both the random measurement errors and the aliasing errors inherent in the observations. Table 1 shows values of $\sigma_\epsilon^2$ estimated by this method for different elements, levels, and seasons. Only station pairs with at least 100 simultaneous observations were used in the computations.

TABLE 2.—*Autocorrelation functions* ($\mu$)

| Element | Month | Level (mb) | Autocorrelation |
|---|---|---|---|
| Zonal wind component ($U$) | January | 850 | $\mu=[1.44\exp(-0.537\rho^{0.802})-0.44]\cos 0.260\rho$ |
| | | 500 | $\mu=[2.70\exp(-0.211\rho^{1.16})-1.70]\cos 0.356\rho$ |
| | | 200 | $\mu=[2.52\exp(-0.270\rho^{0.845})-1.52]\cos 0.292\rho$ |
| | July | 850 | $\mu=[0.895\exp(-2.12\rho^{1.06})+0.105]\cos 0.441\rho$ |
| | | 500 | $\mu=[1.02\exp(-1.71\rho^{1.36})-0.02]\cos 0.190\rho$ |
| | | 200 | $\mu=[1.01\exp(-1.37\rho^{1.36})-0.01]\cos 0.985\rho$ |
| Meridional wind component ($V$) | January | 850 | $\mu=[1.76\exp(-0.447\rho^{1.38})-0.76]\cos -0.361\rho$ |
| | | 500 | $\mu=[1.69\exp(-0.441\rho^{1.40})-0.69]\cos 0.297\rho$ |
| | | 200 | $\mu=[1.97\exp(-0.318\rho^{1.32})-0.97]\cos 0.293\rho$ |
| | July | 850 | $\mu=[1.07\exp(-2.05\rho^{1.53})-0.07]$ |
| | | 500 | $\mu=[1.14\exp(-2.13\rho^{1.80})-0.14]\cos 0.340\rho$ |
| | | 200 | $\mu=[1.16\exp(-2.16\rho^{1.82})-0.16]\cos 0.525\rho$ |
| Temperature ($T$) | January | 850 | $\mu=[1.67\exp(-0.346\rho^{1.43})-0.67]\cos 0.354\rho$ |
| | | 500 | $\mu=[1.13\exp(-0.561\rho^{1.41})-0.13]$ |
| | | 200 | $\mu=[0.94\exp(-0.780\rho^{1.17})+0.06]\cos 0.127\rho$ |
| | July | 850 | $\mu=[0.869\exp(-2.82\rho^{1.06})+0.131]\cos 0.235\rho$ |
| | | 500 | $\mu=[0.774\exp(-1.87\rho^{1.21})+0.226]\cos 0.317\rho$ |
| | | 200 | $\mu=[0.685\exp(-2.19\rho^{0.989})+0.315]\cos 0.215\rho$ |
| Geopotential ($Z$) | January | 850 | $\mu=[0.511\exp(-0.95\rho^{1.6})+0.489]\cos 0.346\rho$ |
| | | 500 | $\mu=[2.91\exp(-0.111\rho^{0.879})-1.91]\cos 0.572\rho$ |
| | | 200 | $\mu=[2.25\exp(-0.208\rho^{0.664})-1.25]\cos 0.566\rho$ |
| | July | 850 | $\mu=[0.915\exp(-0.716\rho^{0.751})+0.085]$ |
| | | 500 | $\mu=[0.841\exp(-1.80\rho^{0.830})+0.159]$ |
| | | 200 | $\mu=[0.842\exp(-1.86\rho^{0.905})+0.158]$ |

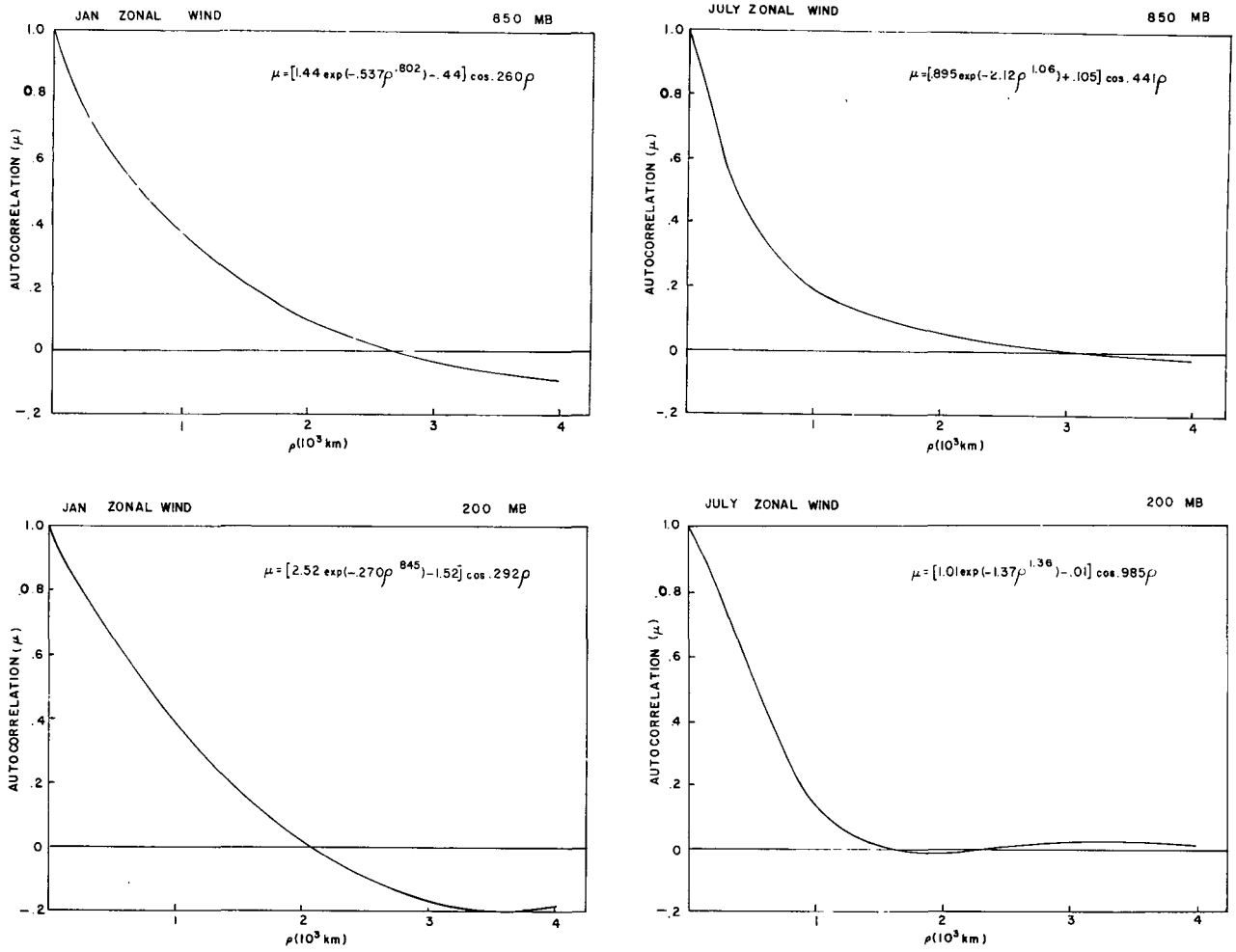


FIGURE 2.—Autocorrelation functions of the zonal component of the wind as a function of distance, $\rho$.

## b. Variances

It is well known that variances computed from data having random errors are too high by an amount equal to the mean-square value of these errors. For the purpose of the present study, the variances were computed at individual stations and corrected by substracting $\sigma_\epsilon^2$ as determined by the procedure described above. The resulting values were, of course, different from station to station. However, to be consistent with the assumptions of homogeneity, the individual values were averaged over all stations for each element, level, and season. These average corrected values are listed in table 1.

## c. Autocorrelation Functions

Under the assumption of homogeneity and isotropy, the autocorrelation, $\mu$, is a function only of the distance, $\rho$, between observation pairs and may be written

$$\mu(\rho)=\frac{\overline{f_i' f_j'}}{\sigma^2}. \tag{14}$$

The average corrected variance was used in the above equation. Again, as in the case of the structure function, only station pairs with at least 100 simultaneous observations were used. The computed autocorrelations, plotted against $\rho$, showed a certain amount of scatter, partly as a result of the anisotropy and nonhomogeneity of the true autocorrelations. We divided this scatter of points into 100-km segments with middle points located at a distance $d=150, 250, 350, \ldots, 3950$ km and determined values of $\mu(d)$ in each interval by means of a function from Petersen and Truske (1969) that weights the computed values in each interval in accordance with the number of events ($N_i$) from which they were determined, and on the basis of their distance from the middle point of their respective intervals. This function is

$$\mu(d)=\sum_{i=1}^{n}\hat{\mu}(\rho_i)\frac{N_i\left[\frac{1}{2}+\frac{1}{2}\cos\frac{\pi(\rho_i-d)}{100}\right]}{\sum_{j=1}^{n}N_j\left[\frac{1}{2}+\frac{1}{2}\cos\frac{\pi(\rho_i-d)}{100}\right]}. \tag{15}$$

In the above equation, $\rho_i$ denotes the distance between pairs of stations used in the calculations and its value for each $d$ ranges between $d+50$ and $d-50$ km.

The values, $\mu(d)$, obtained by the above procedure were then fitted to empirical curves of the form

$$\mu(\rho)=[A\exp(-B\rho^C)+1-A]\cos D\rho. \tag{16}$$

This form was selected because it insures that the fitted autocorrelation functions are positive-definite, as they should be, and that moreover at $\rho=0$, $\mu(\rho)=1$. A "direct-

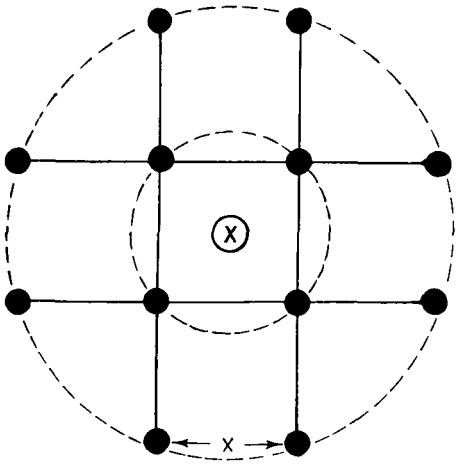


FIGURE 3.—The 12-point interpolation grid used in this study.

search" technique (Hooke and Jeeves 1961) was used to determine the coefficients $A$, $B$, $C$, and $D$. This method consists of making an initial estimate of the coefficients and then modifying these estimates in accordance with a least-squares error test. The testing algorithm changes the coefficients serially at a rate depending on the error reduction effected by each change. Generally, about 350–500 iterations are needed to arrive at the final solution. Almost identical final values of the coefficients are obtained from widely varying initial estimates. The autocorrelation functions derived using this technique are listed in table 2. A selection of the computed autocorrelation curves used in this study are shown in figure 2.

## 4. HOMOGENEOUS OBSERVATIONS

### a. Optimum Weights

The autocorrelation functions play an important role in determining the relative weights to be given to observations at different distances from the location to which the interpolation is made. To demonstrate how the weights vary with different distances and different values of the autocorrelation function, we have used a 12-point interpolation system schematized in figure 3. The interpolation is made to the central point, ⊗, from an inner ring of four observations and an outer ring of eight observations. Figures 4 and 5 show the manner in which the weights of the inner-ring observations; $p_1$, and of the outer-ring observations, $p_2$, vary as a function of the exponent, $A$, of an assumed autocorrelation function, $\mu=e^{-A\rho}$. The value of $A$ roughly defines the scale of the field; the larger it is, the smaller the scale. Figures 4 and 5 are identical except for $\lambda$, which is assumed to be 0.19 in figure 4 and 0.53 in figure 5.

The figures show that, when $A$ is large, $p_1$ rises to a maximum when $x$ is relatively small and starts to decrease thereafter. As $A$ becomes smaller, $p_1$ reaches its maximum value at a larger grid length. For a given value of $\lambda$, the maximum value of $p_1$ is constant. However, the smaller $\lambda$ is the larger this maximum value. For equal values of $A$, the value of $x$ corresponding to the maximum value of

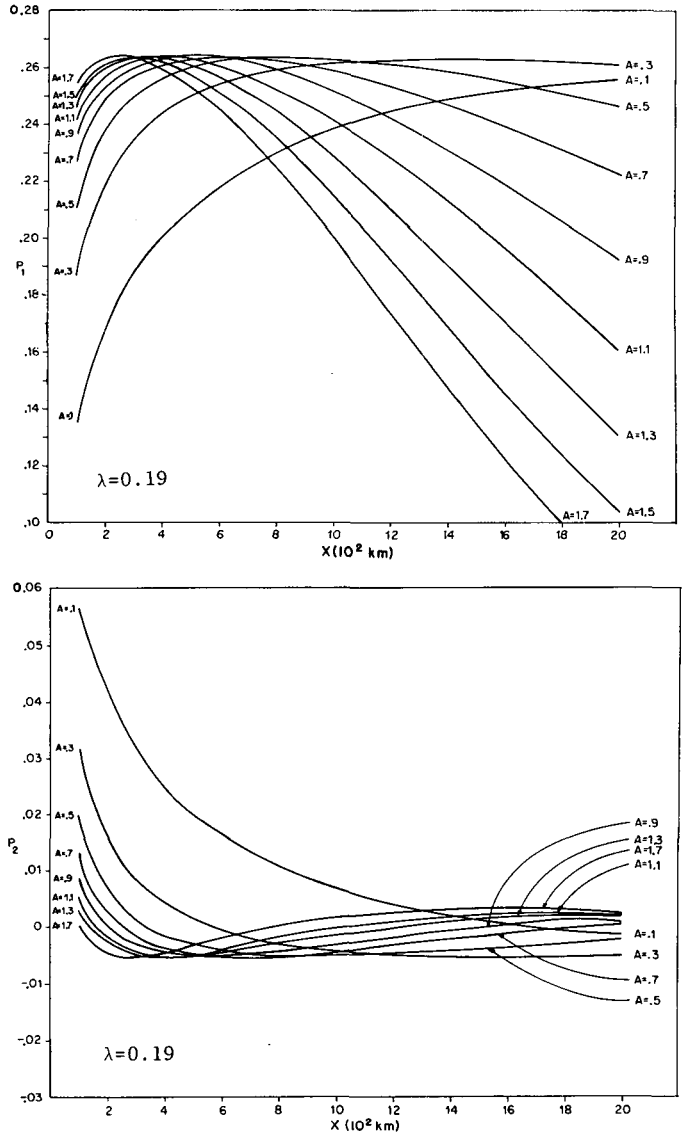


FIGURE 4.—The variation with grid length, $x$, of the optimum weights of inner-ring and outer-ring observations ($p_1$ and $p_2$, respectively) in the 12-point interpolation scheme of figure 3 as a function of the exponent, A, of an assumed autocorrelation function, $\mu=e^{-A\rho}$. A value of $\lambda=0.19$ is assumed.

$p_1$ is larger for larger values of $\lambda$. Note that when $\lambda$ is comparatively small, $p_2$ increases as a function of $x$ when $p_1$ decreases and vice-versa. However, when $\lambda$ is large, both sets of weights can decrease simultaneously with increasing $x$, indicating a rapid increase in the error of interpolation with decreasing observational density.

Figure 6 illustrates how optimum weights vary with locality and season even when the random errors of observation are assumed to be constant. The solid curves represent the weights appropriate to an autocorrelation function, $\mu=e^{-1.8\rho}$, which approximates conditions in the Caribbean region for the 500-mb geopotential field in July. The dashed curves are appropriate to an autocorrelation function, $\mu=e^{-0.14\rho}$, which is more representative of conditions in extratropical regions in January (Alaka 1970). The marked difference in weights, especially those relating to the closer observations, $p_1$, clearly in-

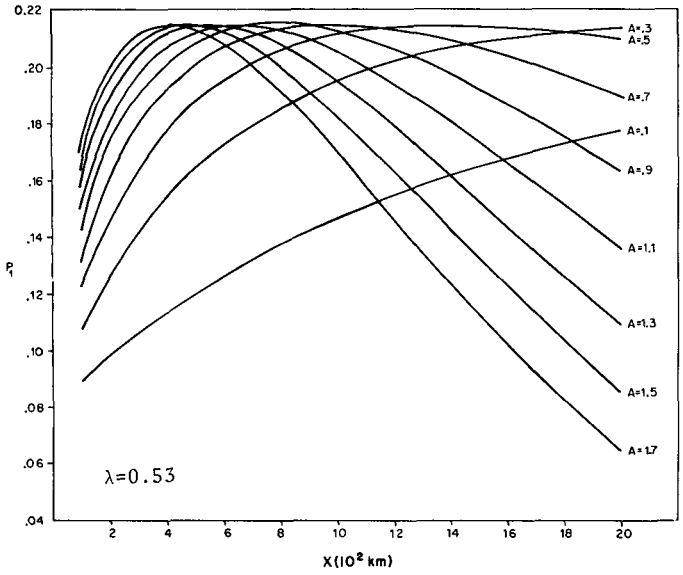


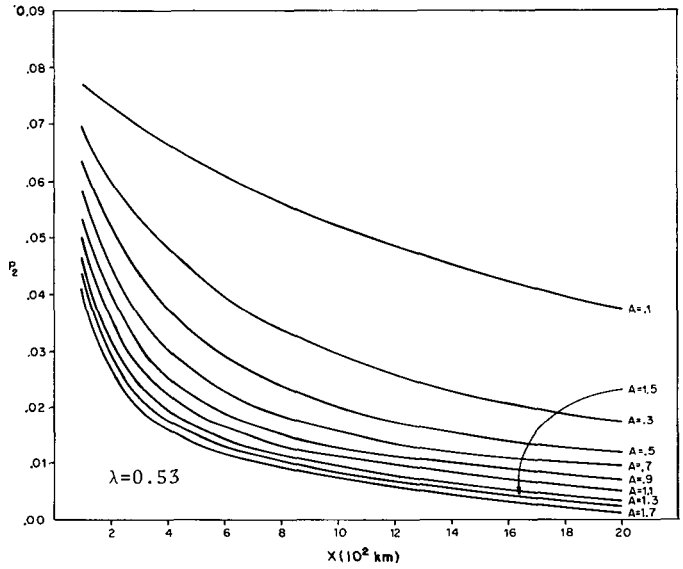


FIGURE 5.—Same as figure 4 for $\lambda = 0.53$.

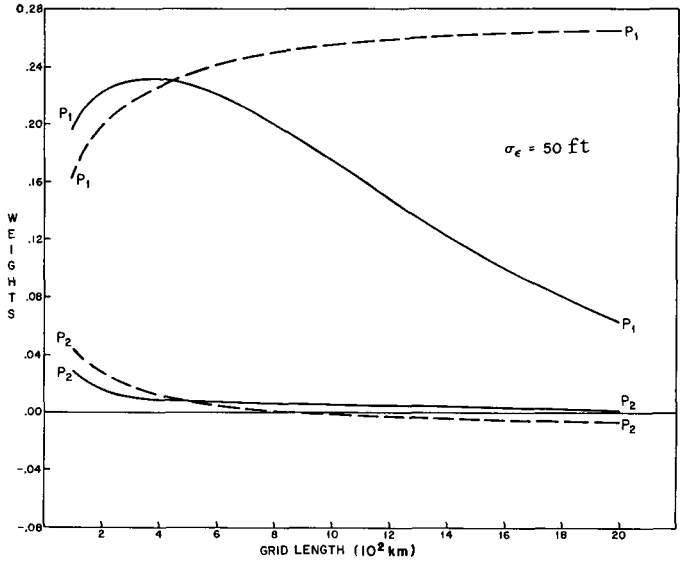


FIGURE 6.—Optimum interpolation weights of inner-ring observations, $p_1$, and outer-ring observations, $p_2$, for the 500-mb geopotential field in the Caribbean in July (solid curve) and in Northern Hemisphere extratropical regions in January (dashed curve).

dicates that an interpolation scheme that may be satisfactory for one region and season may be less than satisfactory for another region and season.

## b. Errors of Optimum Interpolation

We have used eq (10) and (11) to determine the accuracy with which we can estimate the value of the zonal wind component, $U$, at a central point by optimum interpolation from the nearest 12 observations located on a regular grid as shown in figure 3. The rms random errors and variances from table 1 and the autocorrelation functions from table 2 were used in the computations.

Figures 7A and 7B show the rms interpolation errors of $U$ in January as a function of the rms random error, $\sigma_\epsilon$, and the grid length, $x$. The curved dashed line is the locus of points where the rms interpolation error $E^{1/2} = \sigma_\epsilon$. Below this line, the interpolation errors exceed the rms random errors; above the line, the interpolated values are more accurate than the observations used in the interpolation. The less accurate the observations and the closer together they are, the more the gain in accuracy achieved by the interpolated values over the raw observations. The horizontal dashed lines in the figures indicate the estimated present level of the rms random errors of rawin observations at the respective levels. They indicate that the observational grid length must be less than 100 km to obtain interpolated values more accurate than the raw observations.

Comparison of figures 7A and 7B shows that, for the same grid length, the present rawin observations are associated with higher rms interpolation errors at 200 mb than at 850 mb. However, if we consider a normalized error criterion $Q = E^{1/2}/\sigma$, the reverse is true. This reversal is a result of the higher standard deviation of the zonal wind at 200 mb than at 850 mb and is illustrated in figure 8, which shows the distribution of $Q$ at 850 and 200 mb in January as a function of $\sigma_\epsilon$ and the number of regularly spaced observations in a zonal strip between 30°N and 30°S. The scale at the top of the figures shows the distance between observations. Figure 9 shows the distribution of $Q$ in July.

A common feature of figures 8 and 9 is that, near the present level of the random errors of rawin observations (indicated by the dashed horizontal line), the isopleths of $Q$ are almost vertical when the station separation is large. This indicates that decreasing the separation between observations is much more effective in reducing the errors of interpolation than increasing the accuracy of observation. Indeed, at 850 mb, if the distance between neighboring observations is about 800 km or more, it makes very little difference to the accuracy of the interpolated values whether the random errors of observations are 2 kt or twice that amount. At 200 mb, the range of observational errors associated with comparable interpolation errors is even larger when the station separation is large. Under these circumstances, there would seem to be very little point

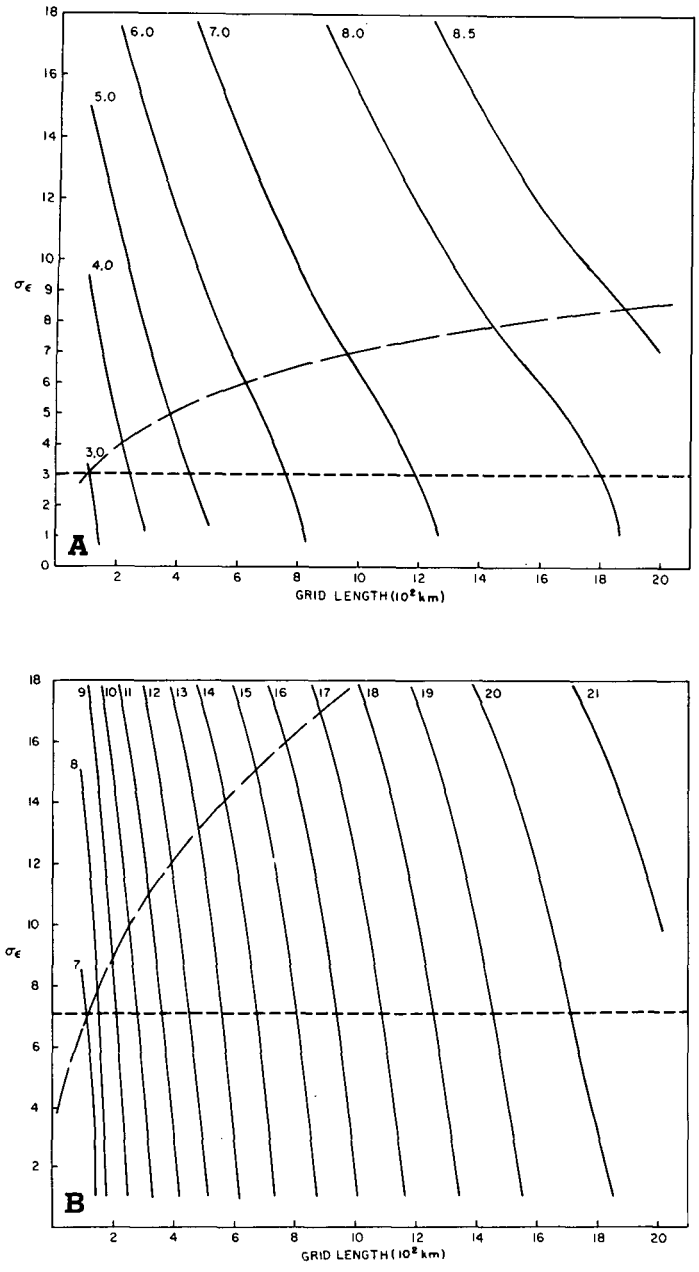


FIGURE 7.—Rms interpolation errors, $E^{1/2}$, of the zonal wind in January as a function of the rms random observation error, $\sigma_\epsilon$, and grid length, $x$, at (A) 850 mb and (B) 200 mb. The dashed curves are the locus of points where $E^{1/2}=\sigma_\epsilon$. The dashed straight lines indicate the estimated present level of the rms random errors of rawin observations.

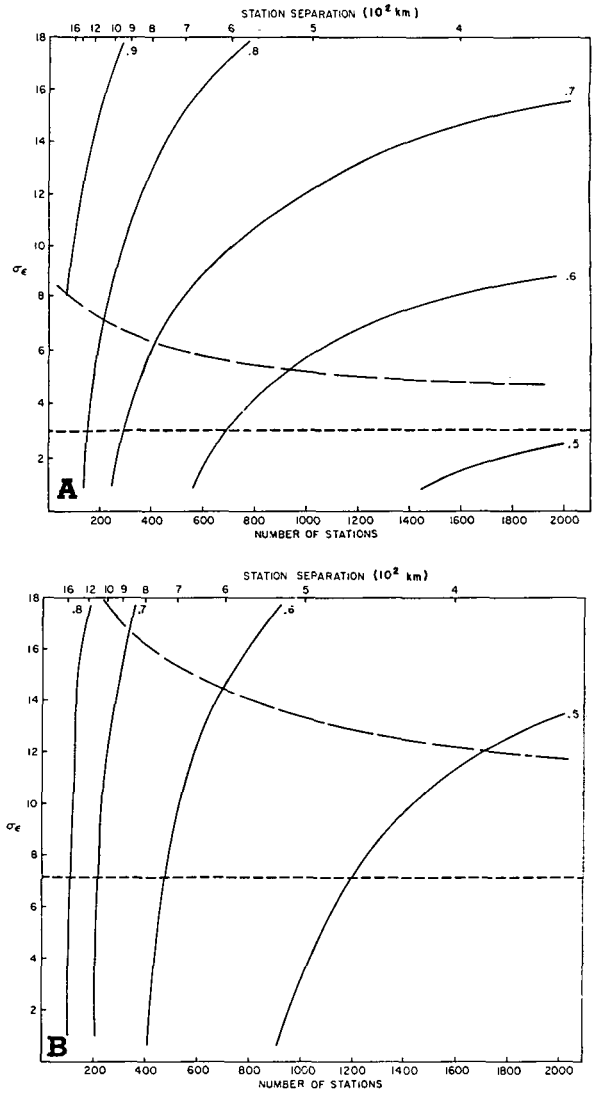


FIGURE 8.—Normalized rms interpolation errors, $Q=E^{1/2}/\sigma$, of the zonal wind in January as a function of the rms observation errors and the number of observations in a tropical belt from 30°N to 30°S at (A) 850 mb and (B) 200 mb. The dashed curves are the locus of points where $Q=\sigma_\epsilon/\sigma$. The dashed straight lines indicate the estimated present level of the rms random errors of rawin observations.

in attempting to provide very accurate observations, especially if these involve added effort and expense.[2]

As the station separation decreases, the isolines of $Q$ tend to curve until they become quasi-horizontal when the grid distance is reduced, say to 400 km or less. Beyond this point, very little improvement is achieved by further reducing the station separation. By the same token, any increase in the accuracy of interpolation can be achieved almost exclusively by increasing the accuracy of the raw observations.

[2] According to a recent study by Steinitz et al. (1970), this conclusion may not be valid for temperature and geopotential fields in the Tropics.

## c. Network Considerations

Figure 10 shows the variation of the rms interpolation errors of the zonal wind component as a function of the number of regularly spaced observations over the tropical zone between 30°N and 30°S. The scale at the top of the figure indicates the corresponding distance between observations in hundreds of kilometers. The estimated random errors of current rawin observations listed in table 2 have been used in the computations.

As one would expect, figure 10 clearly shows that, when the number of observations is small, a comparatively large gain is achieved by increasing the number of observations. As these observations become denser, the gain achieved from a given number of additional observations decreases progressively. Thus, at 200 mb in January, the rms interpolation error may be reduced by 4 kt, from 18 to 14 kt, by increasing the number of observations from

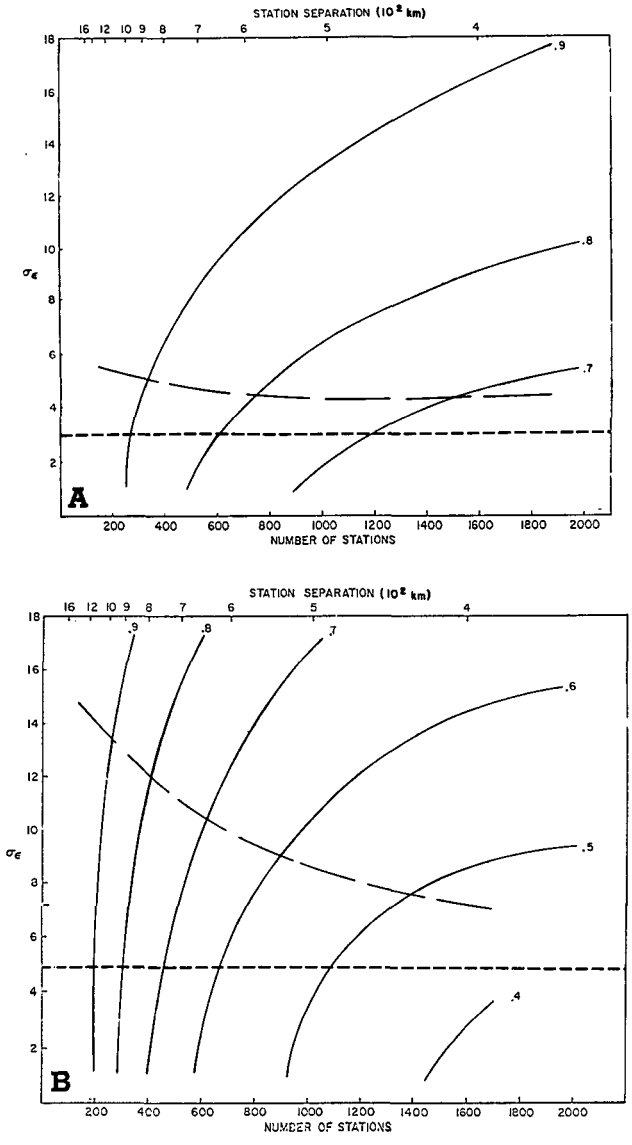


FIGURE 9.—Same as figure 8 for July.

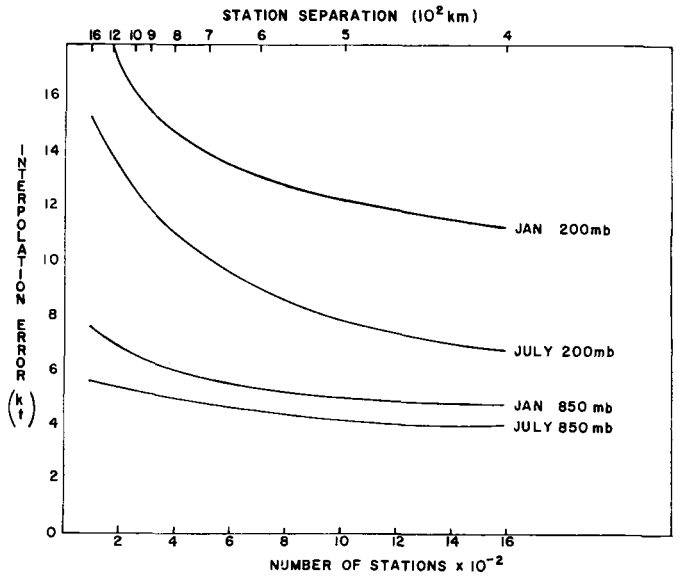


FIGURE 10.—Rms errors of optimum interpolation of the zonal wind from current rawin observations as a function of grid spacing.

about 200 to 550 (i.e., by decreasing the distance between neighboring observations from 1200 to 700 km). However, a further addition of 500 observations would reduce the interpolation error by less than 2 kt. Beyond that, an increase of 600 additional observations would further reduce the interpolation error by less than 1 kt. A similar trend is noticeable at 200 mb in July. At 850 mb, the curves are more flat indicating a smaller rate of gain in accuracy resulting from a given increase in the density of observations.

The point of diminishing returns cannot be determined objectively. It depends on the purpose for which the observations are intended and the economic or scientific benefits of a given increment of accuracy in comparison with the effort and expense involved in providing the additional observations required to achieve this accuracy. For the purposes of forecasting by numerical models, the point of diminishing returns may be estimated by running these models with different data inputs and determining the manner in which the accuracy of forecasts is affected by increasing or decreasing the density of observations (Alaka and Lewis 1967, 1969, Gandin et al. 1967). However, the results of such experiments depend not only on the model used but also on the season, location, and meteorological situation.

## 5. NONHOMOGENEOUS DATA

The procedure symbolized in eq (10) and (11) can accommodate nonhomogeneous data as long as their error statistics are known. Each observation is given an appropriate weight depending on its error and on its position with respect to other observations and to the point to which the interpolation is made. The nonhomogeneous data may be synoptic observations of different quality, a mixture of synoptic and asynoptic observations, or a mixture of observations and forecasts.

### a. Observations of Mixed Quality

Table 3 shows the effect on the rms interpolation error of the 850-mb zonal wind in January at the center of a 12-point grid where a varying number of "good" observations are replaced by observations with three times their rms error. The manner in which good and bad observations are mixed is indicated in the configurations at the top of each column. The values of $\sigma_\epsilon$ in the first column are those of the better observations denoted by dots, while the crosses indicate the locations of the less accurate observations. Thus, in the top row of table 3, a dot denotes an observation with an rms random error of 1 kt while a cross denotes an observation with an rms random error of 3 kt. For the sake of comparison, the table also shows the rms interpolation errors from only four good observations (configuration A) and from 12 good observations (configuration B).

Comparison of the rms errors under configuration A in table 3 with those under configurations B–J indicates that when the rms random errors are very small (1 kt) there is little or no advantage in using other than the four closest

TABLE 3.—*Rms interpolation errors of the zonal wind at 850 mb in January, associated with different configurations of observations of mixed quality. Values of $\sigma_\epsilon$, denoted by dots, represent the better observations; xs represent observations with rms of $3\sigma_\epsilon$.*

| $\sigma_\epsilon$ (kt) | A | B | C | D | E | F | G | H | I | J | K | L | M | N |
|---|---|---|---|---|---|---|---|---|---|---|---|---|---|---|
| | | | | | | Gridlength = 200 km | | | | | | | | |
| 1 | 3.510 | 3.510 | 3.510 | 3.510 | 3.510 | 3.510 | 3.510 | 3.510 | 3.510 | 3.510 | 3.559 | 3.614 | 3.671 | 3.737 |
| 3 | 3.789 | 3.741 | 3.743 | 3.745 | 3.748 | 3.750 | 3.753 | 3.755 | 3.758 | 3.761 | 3.852 | 3.991 | 4.146 | 4.348 |
| 5 | 4.238 | 4.041 | 4.051 | 4.065 | 4.079 | 4.096 | 4.111 | 4.127 | 4.143 | 4.168 | 4.164 | 4.316 | 4.485 | 4.700 |
| | | | | | | Gridlength = 400 km | | | | | | | | |
| 1 | 5.333 | 5.333 | 5.333 | 5.333 | 5.333 | 5.333 | 5.333 | 5.333 | 5.333 | 5.333 | 5.372 | 5.414 | 5.456 | 5.502 |
| 3 | 5.521 | 5.503 | 5.503 | 5.504 | 5.505 | 5.505 | 5.506 | 5.507 | 5.507 | 5.508 | 5.636 | 5.802 | 5.981 | 6.209 |
| 5 | 5.832 | 5.764 | 5.767 | 5.773 | 5.778 | 5.784 | 5.788 | 5.794 | 5.798 | 5.805 | 5.929 | 6.137 | 6.368 | 6.666 |
| | | | | | | Gridlength = 1000 km | | | | | | | | |
| 1 | 6.448 | 6.447 | 6.447 | 6.447 | 6.447 | 6.447 | 6.447 | 6.447 | 6.447 | 6.447 | 6.481 | 6.516 | 6.552 | 6.589 |
| 3 | 6.611 | 6.590 | 6.590 | 6.590 | 6.590 | 6.591 | 6.591 | 6.591 | 6.591 | 6.592 | 6.726 | 6.892 | 7.068 | 7.286 |
| 5 | 6.845 | 6.820 | 6.822 | 6.824 | 6.826 | 6.828 | 6.830 | 6.832 | 6.833 | 6.836 | 7.000 | 7.224 | 7.470 | 7.784 |

observations in the interpolation. As the rms random errors become larger (3–5 kt), it becomes advantageous to supplement the close observations with more remote observations even if some or all of the latter are of poorer quality (configurations B–J). This is especially the case if the sampling density is relatively high (200-km grid length).

However, it is hard to compensate for bad observations that are close to the point to which the interpolation is made by using more remote observations, even if these are of good quality. For instance, four good, close observations are associated with less rms interpolation errors than 12 observations of which two inner-ring observations are bad (configuration L). Indeed, in all except one combination shown in table 3, namely, when $\sigma_\epsilon=5$ kt and the grid length is 200 km, even one bad inner-ring observation can upset the advantage of eight additional good observations (configurations A vs. K).

An interesting feature of table 3 is that the effects discussed above are relatively small. Compare, for instance, configuration B for $\sigma_\epsilon=1$ kt with configuration N for $\sigma_\epsilon=5$ kt. The difference in the rms interpolation errors associat ed with these two extreme cases is about 1.2 kt when the grid length is 200 km. On the other hand, the increase in the rms interpolation error is more than 1.7 kt where the grid length for configuration B increases to 400 km. This means that it is more advantageous to have a mixture of ob servations 200 km apart, with rms errors ranging from 5 to 15 kt, than to have the same number of observations 400 km apart with rms error of only 1 kt.

The above results are of considerable importance. They point to the good use that can be made of nonconventional

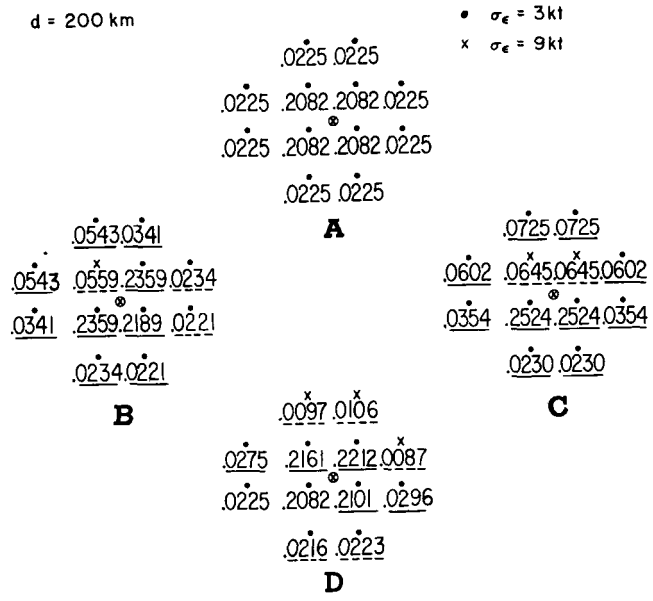


FIGURE 11.—Optimum interpolation weights associated with different configurations of observations of mixed quality. The optimum interpolation is made to the central point ⊗. The good observations (●) have an rms error of 3 kt; the bad observations (X) have an rms error of 9 kt. The solid (dashed) underlines indicate weights which have increased (decreased) from their values in configuration A.

observations such as observations from satellites, which have a high density but are of a relatively poor quality. This, of course, is contingent upon giving these observations their proper weight in relation to other observations. Figure 11 shows the effects on weights arising from increas-

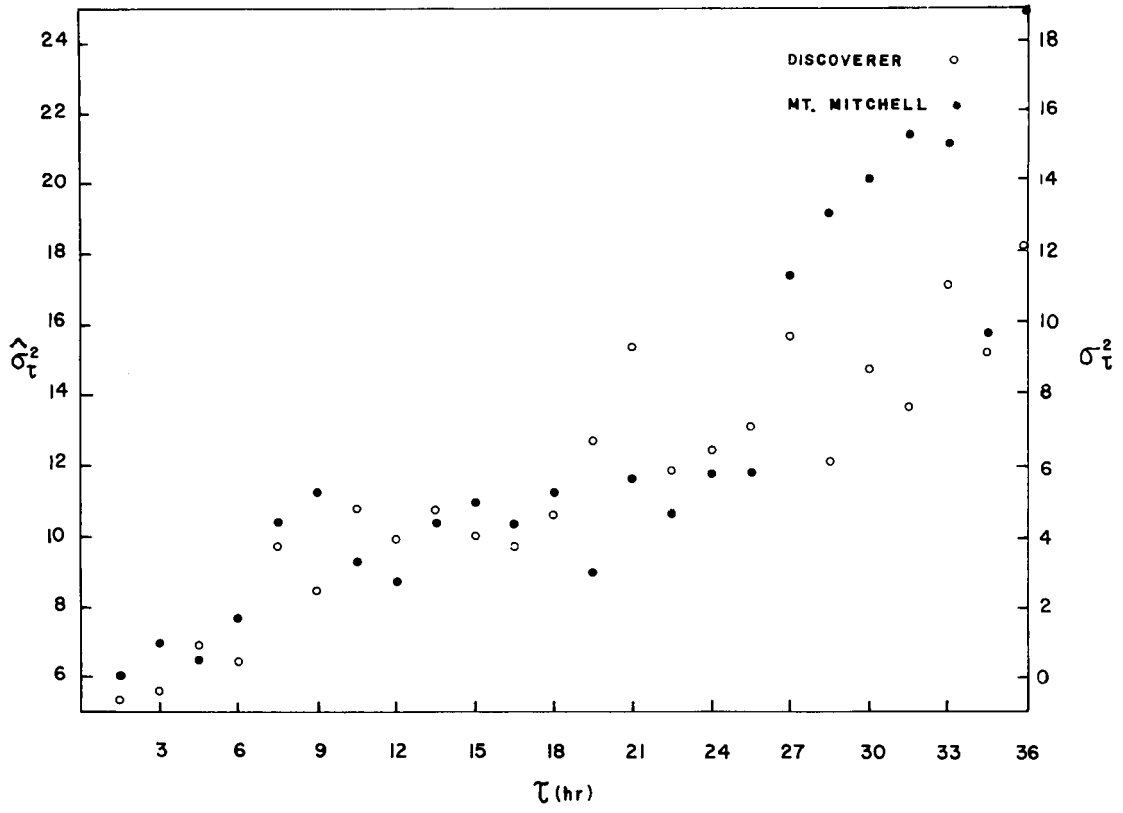


FIGURE 12.—The variation of $\sigma^2_\tau$ of the zonal wind at 850 mb as a function of the time-interval, $\tau$. The left-hand scale relates to the uncorrected values $\hat{\sigma}^2_\tau$; the right-hand scale shows the corrected values $\sigma^2_\tau$.

ing the rms error of one, two, and three observations, in different locations, from 3 to 9 kt. Note that a change in the quality of even one inner-ring observation affects the weight of all observations used in the interpolation.

## b. Asynoptic Observations

The inclusion of asynoptic observations in an optimum interpolation scheme depends on a knowledge of the time-variation of the meteorological element in question.

Consider two sets of observations separated by a time-interval, $\tau$, and let the variance of the change in the value of the observations during this interval be denoted by $\sigma^2_\tau$. This quantity is the temporal equivalent of the structure function, $\beta(\rho)$, discussed in section 3.

In extending the theory of optimum interpolation to accommodate asynoptic observations, we may consider $\sigma^2_\tau$ as an additional source of random errors. Being independent of the random errors of observations, $\sigma^2_\tau$ may be added to the variance of these errors. Thus, a new "effective" rms random error, $\sigma'_\epsilon$, may be written

$$\sigma'_\epsilon=(\sigma^2_\epsilon+\sigma^2_\tau)^{1/2}. \tag{17}$$

If the natural variance, $\sigma^2$, of the element is constant over the interval $\tau$, the quantity $\sigma^2_\tau$ is related to the time-lag autocorrelation coefficient as follows:

$$\sigma^2_\tau=2\sigma^2[1-\mu(\tau)]. \tag{18}$$

To obtain $\sigma^2_\tau$ and $\mu(\tau)$, we had recourse to observations from the Barbados Oceanographic and Meteorological Experiment (BOMEX). In particular, we examined serial rawin ascents from stationary ships participating in the experiments and decided to combine the data from the NOAA ships *Mt. Mitchell* and *Discoverer;* these data appeared to be mutually consistent. The ascents were made in 1969 during the periods May 1–15, May 24–June 10, June 21–July 2, and July 11–July 28.

Figure 12 shows the variation of $\sigma^2_\tau$ of the zonal wind component at 850 mb as a function of the time intervals, $\tau$. The figure has two scales on the ordinate. The left-hand scale relates to the computed values $\hat{\sigma}^2_\tau$. The function that best fitted these values was determined by the direct-search method described in section 3 and was found to be

$$\hat{\sigma}^2_\epsilon=13.7(1-e^{-0.125\tau^{0.32}}\cos 0.432\tau)+6.02. \tag{19}$$

Note that the fitted function has a value of 6.02 at zero time-lag. This quantity represents the inflation of the true values of $\sigma^2_\tau$ arising from the random errors in the data and must be subtracted from the computed values to obtain a corrected estimate. The scale for these corrected estimates is given on the right-hand side of figure 12. The corresponding values of $\mu(\tau)$ are shown in figure 13.

Figure 12 is of considerable interest. It shows that a time-lag of about 24 hr is required for $\sigma^2_\tau$ to equal the mean-square random observation errors, $\sigma^2_\epsilon$, which we have estimated to be approximately 9 kt$^2$. This means that, for the purpose of optimum interpolation, a 24-hr-old rawin observation at 850 mb over the tropical Atlantic during the period May–July is equivalent to a current

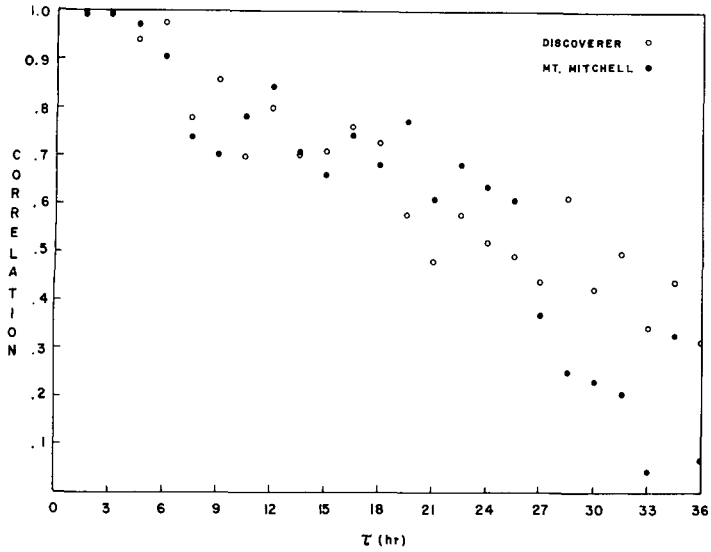


FIGURE 13.—The corrected lag correlation of the 850-mb zonal wind as a function of the time-lag, $\tau$.

observation with twice the mean-square random error. Similarly, an observation that is 6-hr old would be equivalent to a current observation with the mean-square error increased by only about 20 percent. Thus, according to the results of subsections 3b and 3c, replacing a current observation by one that is 6-hr old would result in a relatively small increase in the rms interpolation error.

This conclusion is confirmed by table 4, whichi llustrates the effect of mixing old and new observations on the rms errors of interpolation of the zonal wind at 850 mb in July. We have assumed that the values of $\sigma_\tau^2$ in July are similar to those shown in figure 12, which, as mentioned, were computed from rawin ascents made during a 3-mo period from May to July.

The manner in which old and new observations are mixed is schematized at the top of the table; the new observations are denoted by dots and the old observations by x's. In all cases, the interpolation is made to the central point, ⊗, from 12 surrounding observations as shown. The age of the asynoptic observations, $\tau$, varies from 3 to 24 hr and the grid length of the observational lattice varies from 200 to 1000 km.

From table 4, we note that the increase in the rms interpolation error is almost negligible if all the 12 synoptic observations (configuration A) are replaced by observations which are 3-hr old (configuration E). Indeed, if the grid length of the observational lattice is 200 km, replacing current observations with observations that are even 24-hr old would increase the rms interpolation error from 2.863 to 3.063 kt or about 7 percent. The percent loss becomes even smaller as the grid length of the observational lattice becomes larger. By contrast, if the observational grid length is increased from 200 to 400 km, the rms interpolation error increases by more than 30 percent.

An interesting feature of table 4 is brought out by comparing configurations B and C. These indicate that two old inner observations result in a higher rms interpolation error than four old outer observations. Configuration C also shows that, if the old observations are some distance from the location to which the interpolation is made, it matters very little whether these observations are 3- or 24-hr old.

TABLE 4.—*The effect on the rms interpolation errors of mixing new and old observations in an optimum interpolation scheme of the 850-mb zonal wind. The new observations are denoted by dots. The age ($\tau$) of the old observations is shown in the left-hand column.*

| | A | B | C | D | E |
|---|---|---|---|---|---|
| τ(hr) | 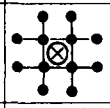 | 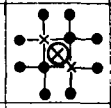 | 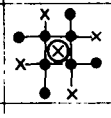 | 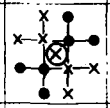 | 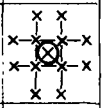 |
| | | Gridlength = 200 km | | | |
| 0 | 2.863 | | | | |
| 3 | | 2.880 | 2.864 | 2.881 | 2.899 |
| 6 | | 2.888 | 2.864 | 2.889 | 2.916 |
| 12 | | 2.905 | 2.864 | 2.907 | 2.956 |
| 24 | | 2.947 | 2.865 | 2.952 | 3.063 |
| | | Gridlength = 400 km | | | |
| 0 | 3.823 | | | | |
| 3 | | 3.837 | 3.823 | 3.837 | 3.853 |
| 6 | | 3.844 | 3.823 | 3.844 | 3.866 |
| 12 | | 3.860 | 3.823 | 3.860 | 3.890 |
| 24 | | 3.900 | 3.823 | 3.901 | 3.993 |
| | | Gridlength = 600 km | | | |
| 0 | 4.479 | | | | |
| 3 | | 4.490 | 4.479 | 4.491 | 4.502 |
| 6 | | 4.496 | 4.479 | 4.496 | 4.513 |
| 12 | | 4.508 | 4.479 | 4.508 | 4.539 |
| 24 | | 4.540 | 4.480 | 4.541 | 4.610 |
| | | Gridlength = 1000 km | | | |
| 0 | 5.228 | | | | |
| 3 | | 5.234 | 5.229 | 5.234 | 5.240 |
| 6 | | 5.237 | 5.229 | 5.237 | 5.245 |
| 12 | | 5.243 | 5.229 | 5.243 | 5.259 |
| 24 | | 5.260 | 5.229 | 5.261 | 5.296 |

## c. Optimum Use of Forecasts

The use of forecasts as an aid to objective analysis is a well-established concept that has proved its merit. The advantage of forecast values is that they are located at gridpoints where they are needed for input into dynamic forecasting models. Obviously, a good observation close to a gridpoint may provide a very good approximation to the gridpoint value and should be given a proportionately large weight in estimating the true gridpoint value. On the other hand, the same observation would be less representative of a more distant gridpoint value and should carry a proportionately smaller weight in estimating that value.

The manner in which observations and forecast gridpoint values may best be combined is a function of the error statistics of both sets of data, of the scale of the meteorological field that is being reconstructed, and of the distance and location of the observations from the gridpoint for which the value is being determined.

In the experiments summarized in figure 14, we have attempted to analyze the rms errors involved in recon-

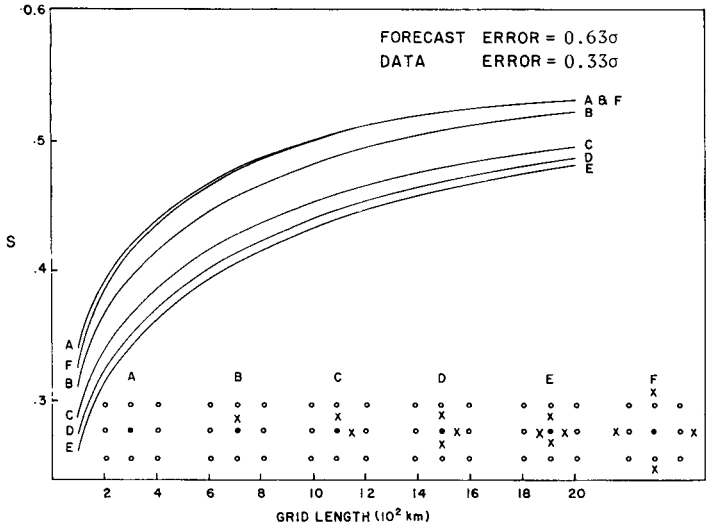


FIGURE 14.—The normalized rms error, $S$, associated with the reconstruction of the zonal wind at 850 mb in January from an eight-point array of forecast gridpoint values interspersed with observations. The solid dots in the configurations at the bottom of the figure denote the location of the reconstructed gridpoint values; the open dots and crosses represent, respectively, forecast gridpoint values and observations used in the reconstruction.

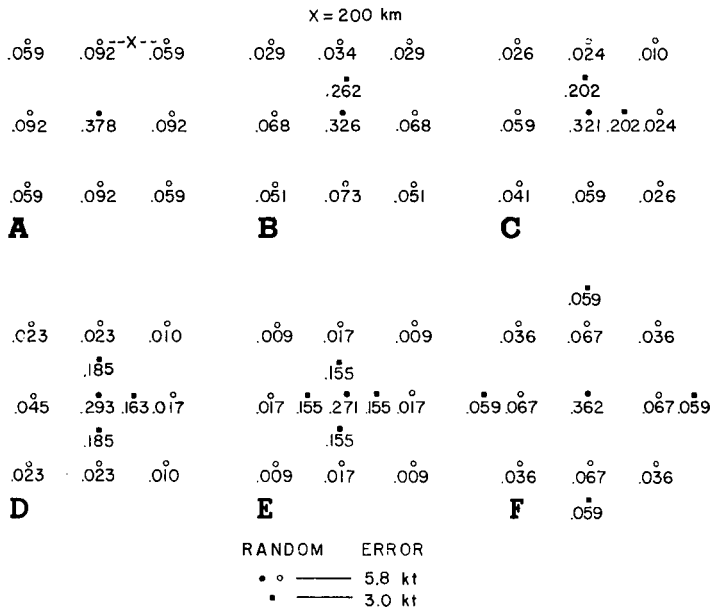


FIGURE 15.—Optimum weights associated with the data configurations of figure 14 when the grid length is 200 km. The open circles denote the gridpoint values that are being reconstructed; the solid dots and squares denote, respectively, the forecast values and the observations used in the reconstruction.

structing the zonal wind field at 850 mb in January from an array of forecast gridpoint values interspersed with observations. We have assumed that the rms error of the observations is 3 kt (i.e., $0.33\sigma$), while the rms error of the forecasts is $0.63\sigma$. In every case, the reconstructed gridpoint value is determined by optimal combination of the forecast value at the gridpoint with the eight nearest gridpoint values plus any observations within two grid lengths of the central gridpoint.

In the experiment schematized in configuration A, we have assumed the absence of new observations and have corrected the central gridpoint value by optimum smoothing with the eight nearest values. The results, shown in curve A, indicate an appreciable reduction in the normalized rms error below that of the unsmoothed forecast value ($S=0.63$), especially if the points in the array are close together. Thus, if the grid length is 300 km, the rms error is reduced from $0.63\sigma$ to $0.42\sigma$. Curves B, C, D, and E show the added improvement that is derived from the introduction of 1, 2, 3, or 4 observations at a distance of one-half grid length in the manner shown in the scheme at the bottom of the figure.

Curve F is of special interest. Comparison with curve A shows that the addition of four observations at a distance of one and one-half grid lengths from the central point is of very little value. Indeed, the rms error in determining the central value does not decrease below that corresponding to optimum smoothing alone, except when the grid length is very small.

Figure 15 shows the optimum weights associated with the data configurations of figure 14 when the grid length is 200 km. The open circles in the figure denote the gridpoint values that are being reconstructed; the solid dots and squares denote, respectively, the forecast values and observations used in the reconstruction. In figure 15A, representative of optimum smoothing, the weight of the central value is slightly more than the combined weights of the four nearest values and slightly less than two-thirds the combined weights of the eight nearest values. A single, good observation as in figure 15B carries more than three-fourths the weight of the central gridpoint value. Its introduction reduces the optimum weights of all the other values used in the interpolation scheme. This reduction is greater for values that are close to the observation. It takes two good observations as in figure 15C to match the weight of the central gridpoint value, even though the rms error of the latter is about two times that of the former. Finally, as shown in figure 15F, the introduction of four distant observations hardly affects the weight of the central value, which remains more than six times larger than that of the individual observations.

## 6. SUMMARY AND CONCLUSIONS

We have attempted to illustrate the manner in which the theory of optimum interpolation can be extended to combine meteorological data from different sources and times into a system that weights each observation in accordance with its relative error characteristics, location, and time of origin. We have shown how the error statistics may be estimated if one disposes of a sufficiently long record of observations. In addition to a knowledge of these random observational errors, the optimality of the theory rests on accurate estimates of the variances and covariances of the meteorological fields that are being reconstructed.

In deriving the basic equations, we found it convenient to make two assumptions. The first, which is generally

valid, is that the random errors are independent of each other and of the true value of the observations. The second and less valid assumption is that the variances are homogeneous and the covariances both homogeneous and isotropic. Because of the latter assumptions and the sensitivity of the experimental results to the autocorrelation values, these results should be considered valid only in a root-mean-square sense, with sizable deviations therefrom to be expected from day to day.

The results reported in sections 4 and 5 relate mainly to the zonal wind component at 850 and 200 mb in January and July. The validity of extrapolating these results to other elements, areas, seasons, and levels will have to be established by further experiments.

It should be stressed that the assumptions of homogeneity and isotropy were made for convenience and are not intrinsic to the basic theory. Given a long enough record of data, it would be possible to compute anisotropic autocorrelations that would be a function of direction, as well as of distance, between observation pairs. Also, at the cost of more computer time, it would be possible to incorporate such anisotropic functions and nonhomogeneous variances into the experiments. Finally, the experiments could conceivably be optimized on a day-to-day basis by computing daily values of $\mu_{i,j}$ from observations used in the interpolation, and $\mu_{0,i}$ from these same observations plus some first-guess value of the element at the point to which the interpolation is made. We highly recommend future experiments that explore the above possibilities.


## ACKNOWLEDGMENTS

The authors are indebted to Brenda Eastridge, Denis Sakelaris, and Darrel Foat of the Techniques Development Laboratory for their capable assistance in the preparation of the manuscript.


## REFERENCES


Alaka, Mikhail A., "Theoretical and Practical Considerations for Network Design," *Meteorological Monographs*, Vol. 11, No. 33, Oct. **1970**, pp. 20–27.

Alaka, Mikhail A., and Lewis, Frank, "Numerical Experiments Leading to the Design of Optimum Global Meteorological Networks," *ESSA Technical Memorandum* WBTM TDL–7, U.S. Department of Commerce, Techniques Development Laboratory, Silver Spring, Md., Feb. **1967**, 14 pp.

Alaka, Mikhail A., and Lewis, Frank, "Numerical Experiments Pertinent to the Design of Optimum Aerological Networks," *Proceedings of the WMO/IUGG Symposium on Numerical Weather Prediction, Tokyo, Japan, November 26–December 4, 1969*, Japan Meteorological Agency, Tokyo, Mar. **1969**, pp. V–9—V–18.

Gandin, Lev Semenovich, *Ob"ektivnyĭ analiz meteorologicheskikh poleĭ* (Objective Analysis of Meteorological Fields), Gidrometeorologicheskoe Izdatel'stvo, Leningrad, U.S.S.R., **1963**, 286 pp.

Gandin, Lev Semenovich, Mashkovitch, S. A., Alaka, Mikhail A., and Lewis, Frank, "Design of Optimum Networks for Aerological Observing Stations," *World Weather Watch Planning Report* No. 21, World Meteorological Organization, Geneva, Switzerland, **1967**, 58 pp.

Hooke, Robert, and Jeeves, T. A., "Direct Search Solution of Numerical and Statistical Problems," *Journal of the Association for Computing Machinery*, Vol. 8, No. 2, Association for Computing Machinery, Baltimore, Md., Apr. **1961**, pp. 212–229.

Petersen, Daniel P., and Truske, T. N., "A Study of Objective Analysis Techniques for Meteorological Fields," *Final Report*, Contract No. EE–163(69), University of New Mexico, Albuquerque, Aug. **1969**, 155 pp.

Sasaki, Yoshikazu, "Numerical Variational Method of Analysis and Prediction," *Proceedings of the WMO/IUGG Symposium on Numerical Weather Prediction, Tokyo, Japan, November 26–December 4, 1968*, Japan Meteorological Agency, Tokyo, Mar. **1969**, pp. VII–25—VII–33.

Steinitz, G., Huss, A., Sinai, R., Manes, A., and Alperson, Z., "Optimum Station Network in the Tropics," *Report*, ESSA Contract No. E–267–(68)N, State of Israel, Ministry of Transport, Israel Meteorological Service, Bet-Dagan, May **1970**, 71 pp.

Thompson, Philip D., "Reduction of Analysis Error Through Constraints of Dynamical Consistency," *Journal of Applied Meteorology*, Vol. 8, No. 5, Oct. **1969**, pp. 738–742.



[*Received December 17, 1971; revised March 28, 1972*]